JOURNAL OF GEOPHYSICAL RESEARCH, VOL. 103, NO. B9, PAGES 21,253–21,273, SEPTEMBER 10, 1998

Ten-second Love-wave propagation and strong ground motions in Taiwan

Chau-Huei Chen
Institute of Seismology, National Chung Cheng University, Chia-Yi, Taiwan

Ta-Liang Teng
Department of Earth Sciences, University of Southern California, Los Angeles

Yuan-Cheng Gung
Institute of Seismology, National Chung Cheng University, Chia-Yi, Taiwan

Abstract. Applying the surface-wave Gaussian beam method to a three-dimensional (3-D) structure of Taiwan, we have studied the generation and propagation of short-period (10-s) surface waves in a region of pronounced crustal heterogeneity, especially in a region defined to be at an epicentral distance larger than a few focal depths away, where high-frequency near-field motions are largely attenuated and surface waves are adequately developed. By perturbing the source model as well as the crustal model in an iterative inversion process, we have achieved an excellent fit to the recent strong-motion observations recorded during the Tung-Ao earthquake (June 5, 1994, $M_L = 6.0$) in Taiwan. This allows us to (1) obtain a refined 3-D crustal model of Taiwan from an initial model that was derived from recent tomographic results and, more important, (2) explain the distribution patterns of the strong shaking reported in terms of intensity maps for historical large earthquakes, and predict the long-period strong-motion distribution patterns for future large earthquakes in Taiwan. With an improved 3-D structure, we have gained better insight into short-period surface-wave propagations as they are modified by crustal lateral heterogeneity. Focusing and defocusing are clearly demonstrated. Of particular interest is the Central Mountain Range, a massive Tertiary metamorphic body forming the backbone of Taiwan, that seems to serve as a "divergent lens" for the propagating surface waves, whereas the large sedimentary basin in southwestern Taiwan seems to focus the wavefronts instead. The computed distortions of the propagating surface-wave field due to lateral heterogeneity are correctly reflected by the observations.

1. Introduction

We are interested in the strong-motion field in a region at epicentral distances beyond a few focal depths, where high-frequency near-field motions are largely attenuated and outgoing surface waves are adequately developed. Strong motions in the immediate vicinity of the source area are very complex, due in part to the high-frequency content of the wave motions that interact with the near-surface medium complexities. Because of the rapid attenuation of high-frequency energy with distance, the earthquake damage in this region defined above is often caused by long-period (up to 10-s) strong ground motions that have survived the attenuation and can impact severely on large-dimension structures. In strong-motion seismology, 10-s waves are considered to be "long-period," whereas in global surface-wave studies, 10-s is considered to be "short-period." This type of damage, particularly severe for regions with a high degree of development, is well documented by a number of recent large earthquakes. Notable examples include that of Mexico City due to the 1985 Michoacan earthquake, of San Francisco and Oakland due to the 1989 Loma Prieta earthquake, and of Taipei due to the 1986 Hualien, Taiwan, earthquake. Generally, these long-period motions are particularly damaging to large structures and other large public works; the resulting high damage loss makes this issue a matter of great concern in hazard assessment and mitigation.

In fact, Japan is particularly concerned about these long-period strong motions that are generated by large events along the subduction boundary offshore because of the source proximity to the great metropolitan Kanto basin. For more than 20 years, recordings of large-amplitude long-period strong motions (6–13 s) in the Kanto basin have been reported [*Seo*, 1978; *Kudo*, 1978; *Tanaka et al.*, 1979; *Yokota et al.*, 1986]. *Kudo* [1978] showed that these long-period motions are primarily traveling surface waves. *Kinoshita et al.* [1992] used a strong-motion array in the Kanto basin to estimate the arrival directions and the apparent velocities of the long-period strong motions. Not only can they make a positive identification of the waves being of Love-type, they further point out that the wave approaching direction sometimes deviates substantially from the direction to the epicenter. *Kato et al.* [1993] first successfully applied a surface-wave Gaussian beam method introduced by *Yomogida and Aki* [1985] to explain a set of strong-motion data recorded at Tokyo and Yokohama, excited by an earthquake more than 100 km away near the Izu peninsula, Japan. Using a crustal model of the Kanto basin with appro-

Paper number 98JB00613.
0148-0227/98/98JB-00613$09.00

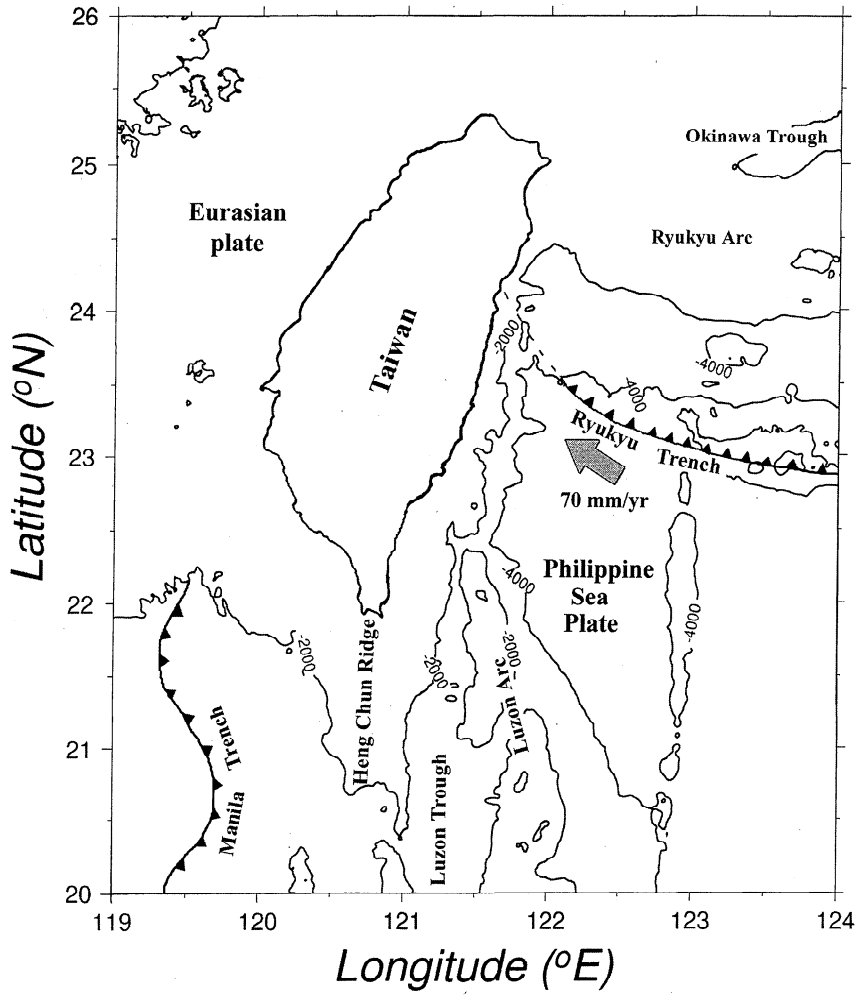

Figure 1. Tectonic setting of Taiwan and neighboring regions. The complicated structure has resulted from the interaction of the Philippine Sea Plate and Eurasian Plate at Taiwan. The Ryukyu Arc system is developed to the east and northeast, and the Luzon Arc system extends to the south (modified from *Ho* [1986]).

priate lateral heterogeneity, they are able to reproduce the arrival times and amplitudes of the recorded Love waves. However, they are not able to synthesize the long duration of the motions. After the 1992 Landers earthquake with as much as 20 cm displacement motions observed in the Los Angeles basin, some 150 km from the source, *Qu et al.* [1994] applied the surface-wave Gaussian beam method to reproduce a large and well-recorded strong-motion data set. In a process of iterative inversion by perturbing a three-dimensional (3-D) southern California crustal model and the source parameters, they are able to reach an excellent fit to the excited Love waves recorded at stations in all azimuths. Their work has clearly demonstrated that the surface-wave Gaussian beam method is suitable and efficient in dealing with problems of surface-wave propagation in laterally heterogeneous medium, and that it is particularly useful in evaluating the strong-motion field in the "long-period region" defined above.

On the west Pacific, Taiwan offers interesting tectonics and crustal heterogeneity for us to further explore the usefulness of this method. Next to a convergent plate boundary, Taiwan has a NNE trending tectonic grain where a high (4000 m) Central Mountain Range of Tertiary age forms the backbone of the island, and a broad Quarternary NNE-elongated sedimentary basin developed on the western slope over the Tertiary basement rocks that form the Central Mountain Range (Figure 1). The crustal structure of Taiwan is reasonably well known through a series of recent seismic wave travel-time analysis [*Tsai et al.*, 1977; *Tsai*, 1978, 1986] and tomographic studies [*Roecker et al.*, 1987; *Chen et al.*, 1994; *Ma et al.*, 1994; *Ho and Shin*, 1994; *Rau and Wu*, 1995]. These results lend themselves conveniently for the construction of an initial 3-D crustal model, which is necessary in order to begin the process of a surface-wave Gaussian beam study. On the Quarternary sediments, most of the important large cities of Taiwan have developed, together with many large-scale public works that, due to the high seismicity, give rise to high seismic risks. Moreover, Taiwan has just completed a period of extensive strong-motion instrumentation program with numerous modern 16-bit digital recorders. Excellent strong-motion data begin to become available; one such set is the recently recorded Tung-Ao earthquake (June 5, 1994, $M_L = 6.0$) that will be used in this study.

2. Methods and Data

By a Mercator projection, surface waves traveling on a spherical Earth are mapped to those traveling in a medium described by 2-D Cartesian coordinates. The Gaussian beam method, originally developed for body waves, can thus be ap-

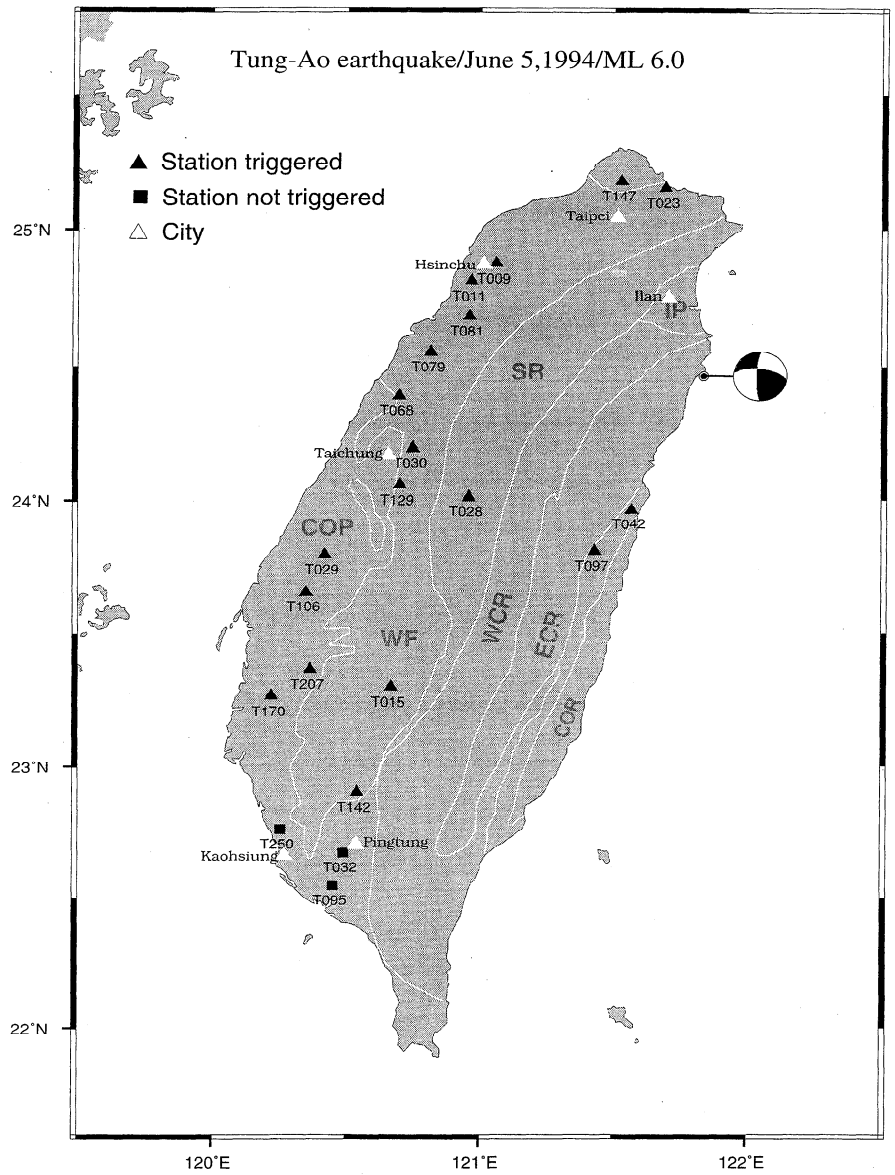

Figure 2. Stations and source locations. Solid triangles represent stations whose records of the Tung-Ao earthquake are used in this study. The three solid squares are stations not triggered during this event. The fault plane solution represents the focal mechanism of the earthquake determined by the Central Weather Bureau of Taiwan. The white curves divide the Taiwan island into geologic regions [*Ho*, 1986]: COP, coastal plain; WF, western foothills; SR, Hsuehshan Range Belt; WCR, western Central Mountain Range; IP, Ilan Plain; ECR, eastern Central Mountain Range; and COR, eastern Coastal Range.

plied to surface waves [*Yomogida and Aki*, 1985, 1987]. *Kato et al.* [1993] and *Qu et al.* [1994] have successfully applied the method of surface-wave Gaussian beam to the Kanto basin in Japan and to southern California, respectively. These four papers, particularly, *Yomogida and Aki*'s [1985], give a comprehensive account of the surface-wave Gaussian beam theory, which will not be repeated here.

Data from the Tung-Ao mainshock (June 5, 1994; M_L = 6.0) are well recorded by 18 stations of the Taiwan Central Weather Bureau Seismic Network (CWBSN), which has 75 stations, each consisting of three-component short-period velocity sensors, and 45 of the stations also have installed three-component force-balance accelerometers. The strong-motion outputs of 18 stations that are more than a few focal depths away (Figure 2) are used in the present study. The force-balance accelerometer has a bandwidth from dc to 50 Hz, a full-scale range of ±2000 Gals, and a dynamic range of 96 dB [*Shin*, 1993]. Signals are digitally recorded at 200 samples/s with a 16-bit analog-to-digital (A/D) converter. Absolute timing is provided by either an Omega clock or a GPS clock. All instruments are shake-table tested at the time of installation and calibrated regularly afterward. Figure 3a gives an example of the acceleration records written by instruments with adequate system response from 0.04 to 15 s. Waveforms have been processed for instrument and baseline corrections, then integrated to obtain displacements (Figure 3b). A Gabor wavelet with central period equal to the dominant period (10 s) found in the spectrum is applied to obtain narrowband displacements (peaked at 10 s) for all stations (Figure 3c). Figure 4 shows samples of band-passed signals and the corresponding dis-

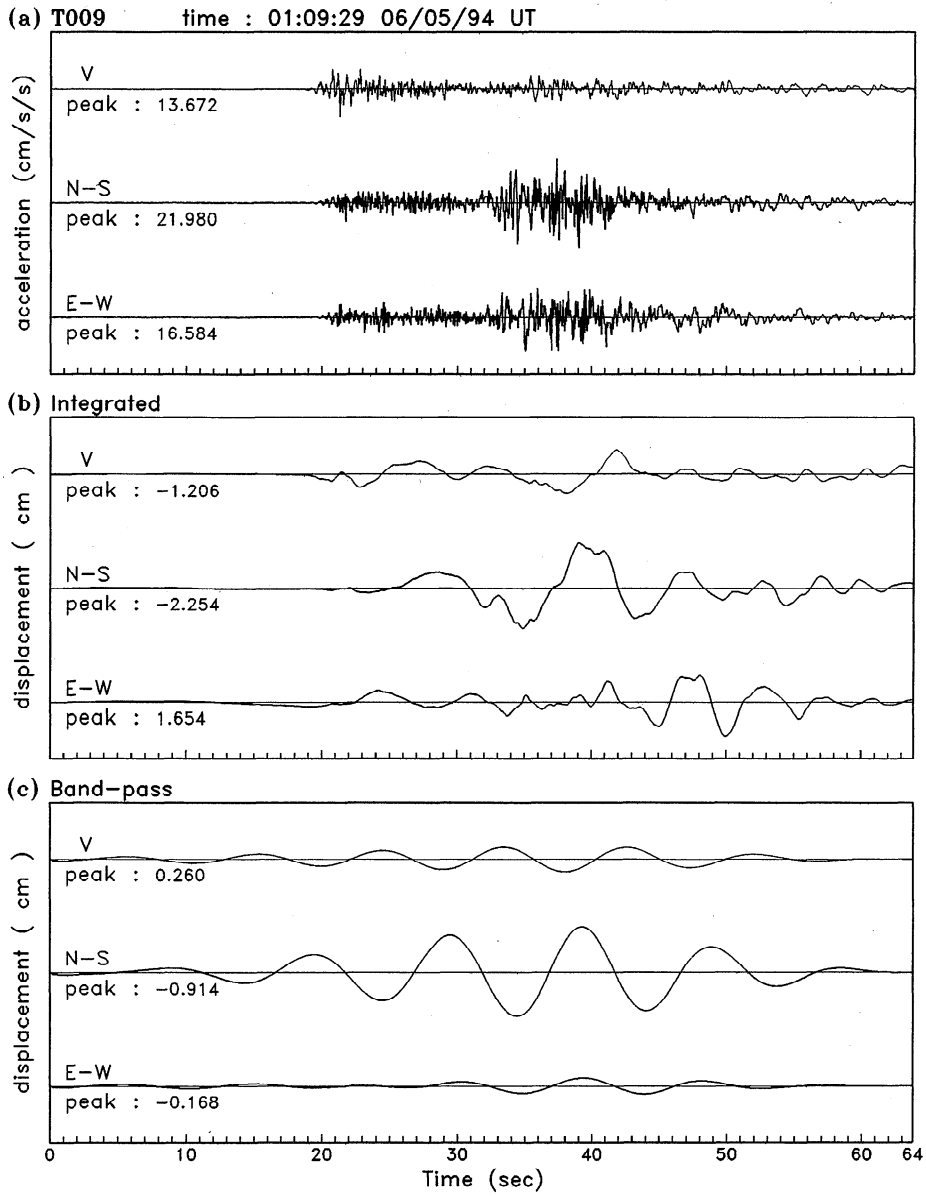

Figure 3. Sample of strong-motion data used: (a) the original three-component acceleration data by station T009, (b) the integrated displacements, and (c) the 10-s period Gabor filtered displacements.

placement spectrums of both horizontal components. It clearly shows in spectrums on the right that the wave energy is concentrated at the period range from 5 to 10 s. Waveforms of horizontal components show dispersive wave trains, and the amplitudes are much larger than those of vertical components (Figure 3a). These characteristics indicate that strong Love waves are excited by the strike-slip source of the Tung-Ao event. To confirm that these wave trains are Love waves, particle trajectories on the horizontal plane for the processed data are drawn with a window length of 35 s after the *S* arrivals (Figure 5). The particle motions show that directions of polarization are roughly perpendicular to the back-azimuths except for some stations with small amplitudes. The small amplitudes are due to these stations' locations near the nodal lines (roughly N40°E and N50°W) derived from the focal mechanism. This fact, along with the result that the vertical components have much smaller amplitudes than those of horizontal components, further confirms that the extracted data around the central period of 10 s are predominantly Love waves as opposed to Rayleigh waves. For better signal-to-noise ratio, this study concentrates on the Love-wave propagation.

3. Crustal Model of Taiwan

In the Taiwan area, many studies have been carried out to determine the velocity distribution for 1-D [*Yeh and Tsai*, 1981] and for 3-D [*Roecker et al.*, 1987; *Ho and Shin*, 1994; *Ma et al.*, 1994; *Rau and Wu*, 1995]. This knowledge of subsurface structures has been improved by various aspects of geophysical and geological studies of the crustal and upper mantle [*Tsai et al.*, 1977; *Tsai*, 1978, 1986]. The *P* wave velocity structures are more commonly available. However, the *S* wave velocity structures and density structures are generally not, and they have to be derived from the *P* wave velocities with an assumed Poisson ratio or through published empirical relations [*Ludwig et al.*, 1970]. A recent *S* wave velocity structure of the Taiwan area

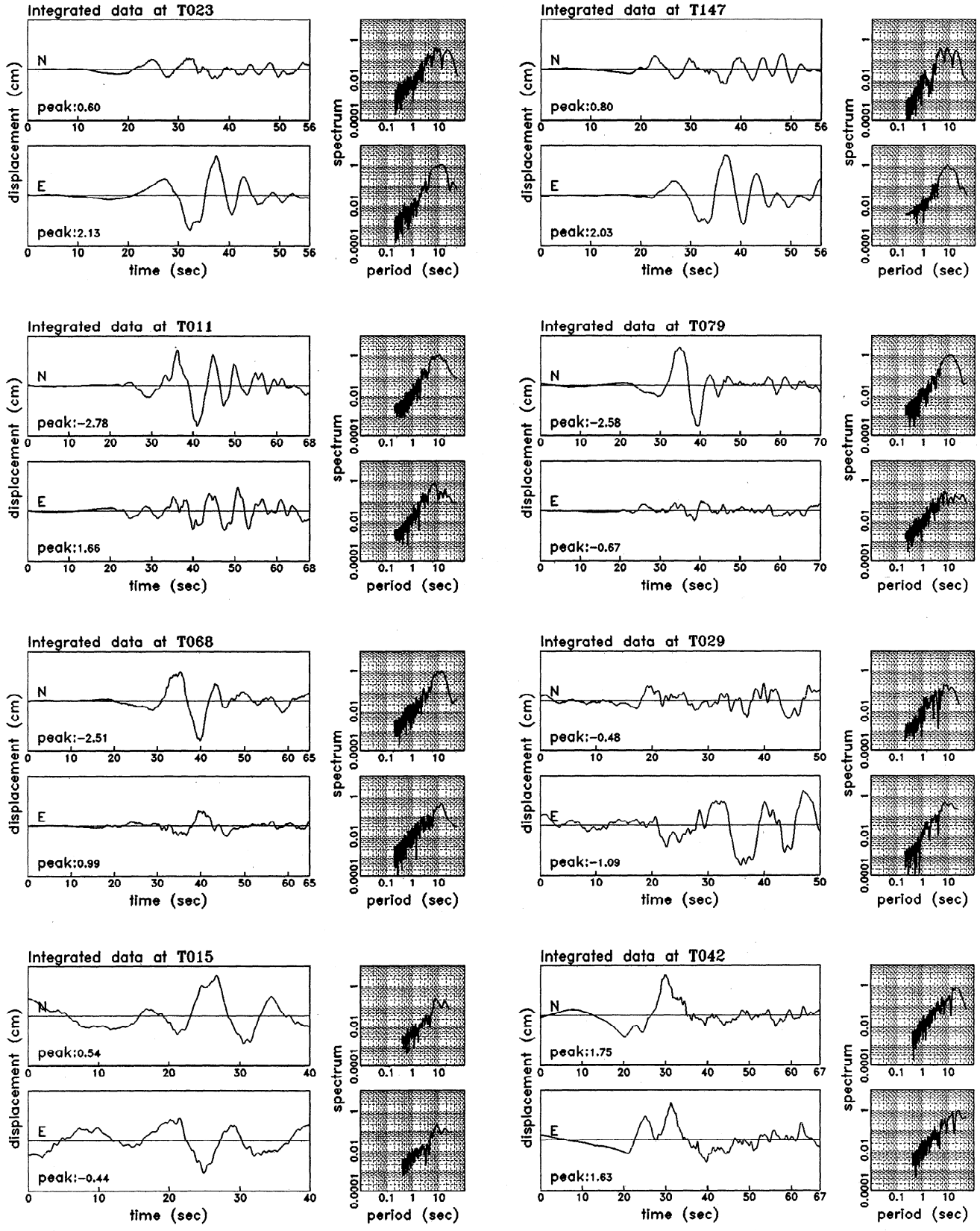

Figure 4. Examples of integrated horizontal displacements and their corresponding spectra used in the current study. This depiction shows that the 10-s period component is dominant for all stations. Note the E-W component of station T023 has much higher spectral amplitude in 10-s period than the N-S component. The reverse is the case for station T011. From the station azimuth, it is clear that Love-like motions are dominant.

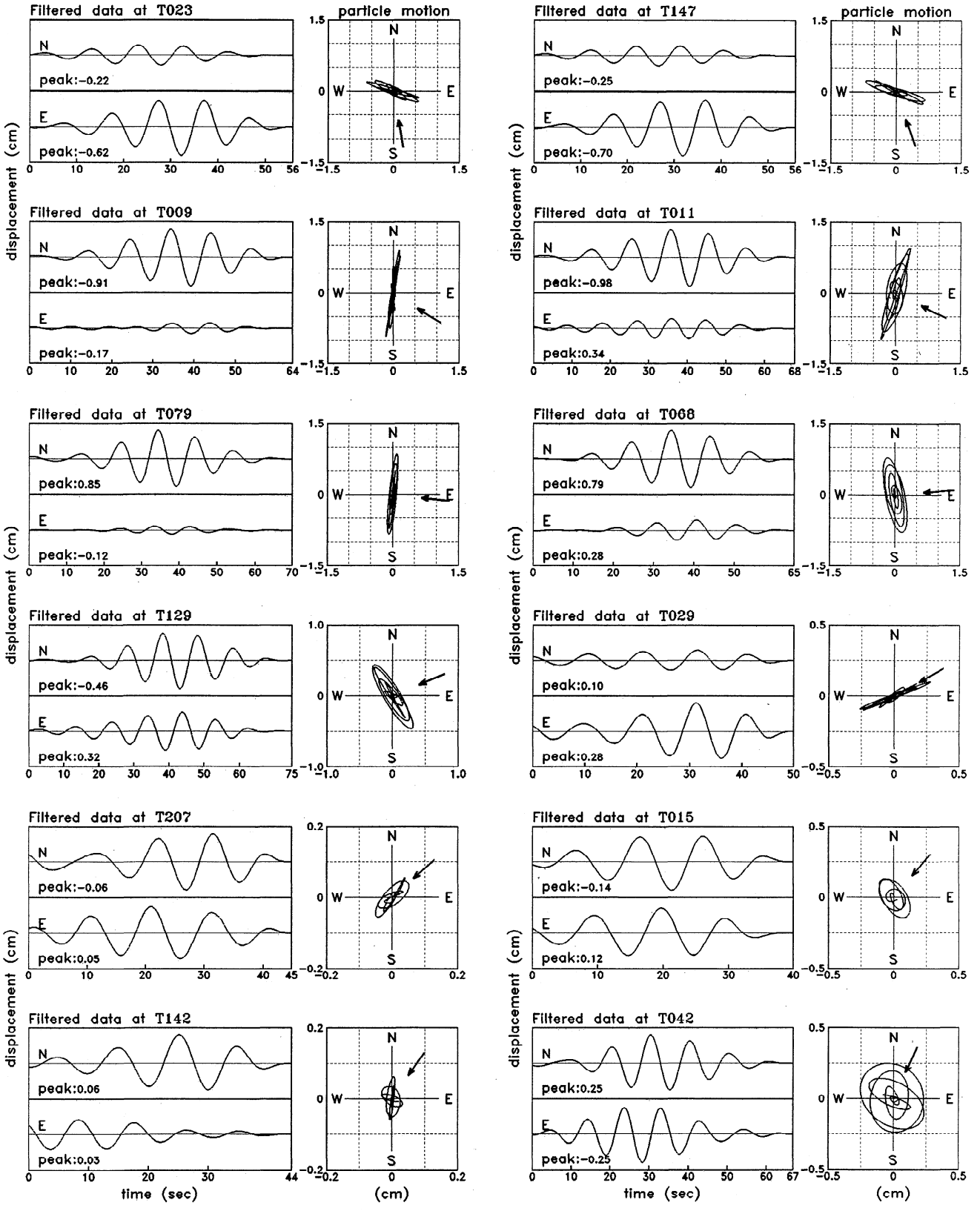

Figure 5. Examples of Gabor band-passed (period 9.5–10.5 s) horizontal displacements and corresponding particle trajectories on the horizontal plane. Arrows denote the orientation of each station to the epicenter.

Table 1. Initial Velocity Models

Model Thickness, km	A		B		C		D		E		F	
	β, km/s	ρ, g/cm^3	β, km/s	ρ, g/cm^3	β, km/s	ρ, g/cm^3	β, km/s	ρ, g/cm^3	β, km/s	ρ, g/cm^3	β	ρ
2.0	2.45	2.40	2.32	2.25	2.64	2.50	2.84	2.50	3.00	2.40	2.26	2.40
3.0	2.56	2.40	2.50	2.45	2.79	2.50	2.93	2.50	3.06	2.45	2.43	2.65
5.0	2.79	2.50	2.86	2.55	3.08	2.52	3.07	2.52	3.29	2.50	2.95	2.65
5.0	3.11	2.60	3.27	2.60	3.28	2.58	3.20	2.58	3.45	2.60	3.68	3.10
10.0	3.55	2.85	3.72	2.90	3.51	2.78	3.38	2.78	3.57	2.80	3.97	3.20
10.0	3.93	3.15	4.11	3.15	3.76	3.06	3.65	3.06	3.89	3.10	4.05	3.20
15.0	4.19	3.30	4.21	3.30	4.06	3.30	3.97	3.30	4.28	3.30	4.15	3.30
	4.35	3.40	4.35	3.40	4.35	3.40	4.34	3.40	4.49	3.40	4.44	3.40

Model Thickness	G		H		I		J		K	
	β	ρ	β	ρ	β	ρ	β	ρ	β	ρ
2.0	2.25	2.40	2.96	2.40	2.86	2.40	2.35	2.40	2.57	2.25
3.0	3.11	2.40	3.08	2.40	2.97	2.40	2.46	2.40	2.67	2.45
5.0	3.33	2.50	3.34	2.50	3.20	2.50	2.75	2.50	2.88	2.55
5.0	3.43	2.60	3.44	2.60	3.49	2.60	3.15	2.60	3.31	2.60
10.0	3.79	2.85	3.53	2.85	3.81	2.85	3.65	2.85	3.72	2.90
10.0	3.96	3.15	3.67	3.15	4.14	3.15	4.14	3.15	4.07	3.15
15.0	4.46	3.30	3.91	3.30	4.29	3.30	4.21	3.30	4.21	3.30
	4.46	3.40	4.28	3.40	4.45	3.40	4.35	3.40	4.35	3.40

Model Thickness	L		M		N		O		P	
	β	ρ	β	ρ	β	ρ	β	ρ	β	ρ
2.0	2.11	2.25	2.20	2.25	2.84	2.50	2.89	2.50	2.84	2.50
3.0	2.20	2.45	2.36	2.45	2.91	2.50	2.94	2.50	2.93	2.50
5.0	2.50	2.55	2.60	2.55	3.02	2.52	3.03	2.52	3.07	2.52
5.0	3.09	2.60	2.88	2.60	3.13	2.58	3.18	2.58	3.27	2.58
10.0	3.61	2.90	3.34	2.90	3.23	2.78	3.45	2.78	3.56	2.78
10.0	4.18	3.15	3.75	3.15	3.39	3.06	3.79	3.06	3.86	3.06
15.0	4.48	3.30	4.17	3.30	3.78	3.30	4.16	3.30	4.18	3.30
	4.49	3.40	4.35	3.40	4.33	3.40	4.35	3.40	4.35	3.40

Model Thickness	Q		R		S		T		U	
	β	ρ	β	ρ	β	ρ	β	ρ	β	ρ
2.0	2.58	2.40	3.05	2.50	2.90	2.40	2.98	2.60	3.01	2.60
3.0	2.72	2.65	3.09	2.50	3.17	2.45	3.12	2.60	3.08	2.60
5.0	3.00	2.65	3.16	2.52	3.40	2.50	3.33	2.60	3.25	2.60
5.0	3.16	3.10	3.24	2.58	3.46	2.60	3.55	2.75	3.51	2.75
10.0	3.29	3.20	3.37	2.78	3.54	2.80	3.79	2.80	3.79	2.80
10.0	3.58	3.20	3.56	3.06	3.71	3.10	4.07	2.70	4.18	2.70
15.0	4.23	3.30	3.86	3.30	4.16	3.30	4.44	3.20	4.47	3.20
	4.49	3.40	4.34	3.40	4.35	3.40	4.49	3.40	4.49	3.40

Model Thickness	V		W		X		Y		Z	
	β	ρ	β	ρ	β	ρ	β	ρ	β	ρ
2.0	2.64	2.55	2.80	2.50	2.39	2.50	2.44	2.40	2.58	2.40
3.0	2.79	2.55	2.92	2.50	2.48	2.50	2.67	2.40	2.72	2.40
5.0	3.14	2.59	3.10	2.54	2.75	2.54	3.02	2.50	3.07	2.50
5.0	3.49	2.62	3.28	2.60	3.15	2.60	3.27	2.60	3.68	2.60
10.0	3.78	2.82	3.65	2.75	3.59	2.75	3.51	2.85	3.99	2.85
10.0	4.18	3.05	4.03	3.00	3.79	3.00	3.95	3.15	4.10	3.15
15.0	4.47	3.20	4.20	3.30	4.02	3.30	4.47	3.30	4.25	3.30
	4.49	3.40	4.35	3.40	4.44	3.40	4.49	3.40	4.47	3.40

Letters A–Z correspond to blocks in Figure 6a. See Figure 6a caption.

[*Chen et al.*, 1994] is derived from utilizing a larger quantity of higher quality of *S* wave arrival times. These results are compiled to construct an initial 3-D structure model of the Taiwan area. The region of study is divided into $0.1° \times 0.1°$ rectangular cells along the longitude and latitude directions. Each cell is assumed to have a laterally homogeneous crustal structure in terms of 1-D *S* wave velocity (Table 1) and density structures (Figure 6a) according to the geological map and our tomographic results mentioned above. The Taiwan region, then, is composed of subregions which are characterized by 26 distinctive velocity models. The surface-wave phase and group velocities for each cell are computed on the basis of this flat-layered

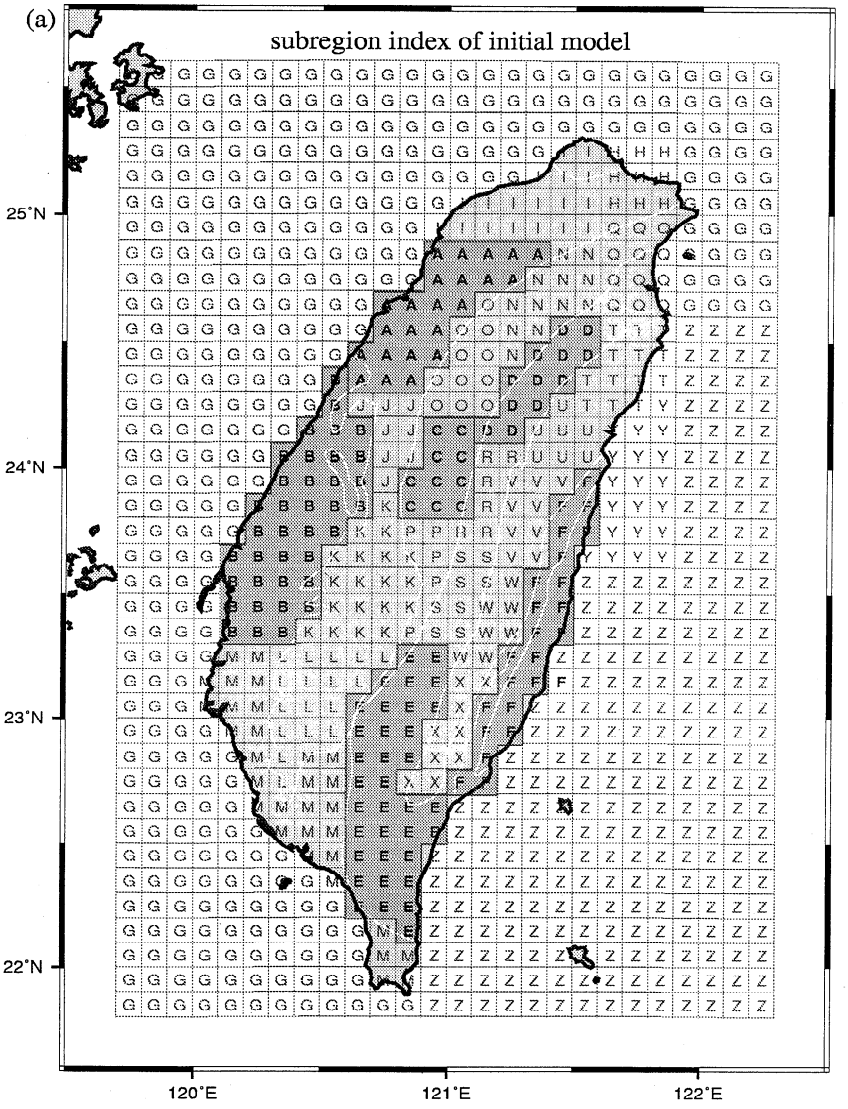

Figure 6a. Initial velocity models. The letters in each block represent different velocity structures (Table 1), which are constructed according to recent geologic and geophysical studies cited in the text.

Earth model using a Thomson-Haskell matrix method. Figures 6b and 6c give corresponding phase and group velocity distributions of the initial model. Note in Figure 6a and Figure 2 that there are three principal structural belts, the eastern Coastal Range (COR), western and eastern Central Mountain Range (WCR and ECR), and coastal plain (COP), reflected in this initial model. By using the bicubic spline interpolation following *Cerveny et al.* [1982], we obtain for a given period smooth surfaces for not only the phase velocity but also its first and second spatial derivatives at each cell. This is important because the second derivative of phase velocity significantly affects the results of the dynamic ray tracing. Meanwhile, a simple linear interpolation is applied to the discrete group velocity. These values are necessary for solving the kinematic and dynamic ray systems. This process of model generation is reasonable for the short-period (~10 s) Gaussian beam surface-wave studies [*Qu et al.*, 1994].

4. Surface-Wave Waveform Modeling

Ray maps from the Tung-Ao source are generated by methods of kinematic and dynamic ray tracing. The interval of takeoff angles is made small enough that the laterally heterogeneous structure is sampled by a finite number of rays, and a sufficiently dense system of rays is generated in order to cover the selected stations. Finally, Gaussian beam contributions for each station are summed according to the values obtained from computations of kinematic and dynamic ray tracing to yield surface-wave synthetics. Several free parameters in the Gaussian beam method are problem oriented, which need to be carefully sorted out by a wide range of numerical tests. According to the results of a sensitivity study on these free parameters for body waves [*Nowack and Aki*, 1984] and for surface waves [*Yomogida and Aki*, 1985], the interval of takeoff angle is chosen to be 0.5°. The range of takeoff angles spanning each station is chosen to guarantee that all significant contributions are included in the construction of the Gaussian beams. In our computations, Gaussian beams with a bell-shaped weighting envelope for each station are summed to yield surface-wave synthetics. The Gaussian beam width is chosen carefully to give an average optimal value for these laterally heterogeneous cases in this study, in a manner thoroughly discussed by *Cerveny and Psencik* [1983a, b].

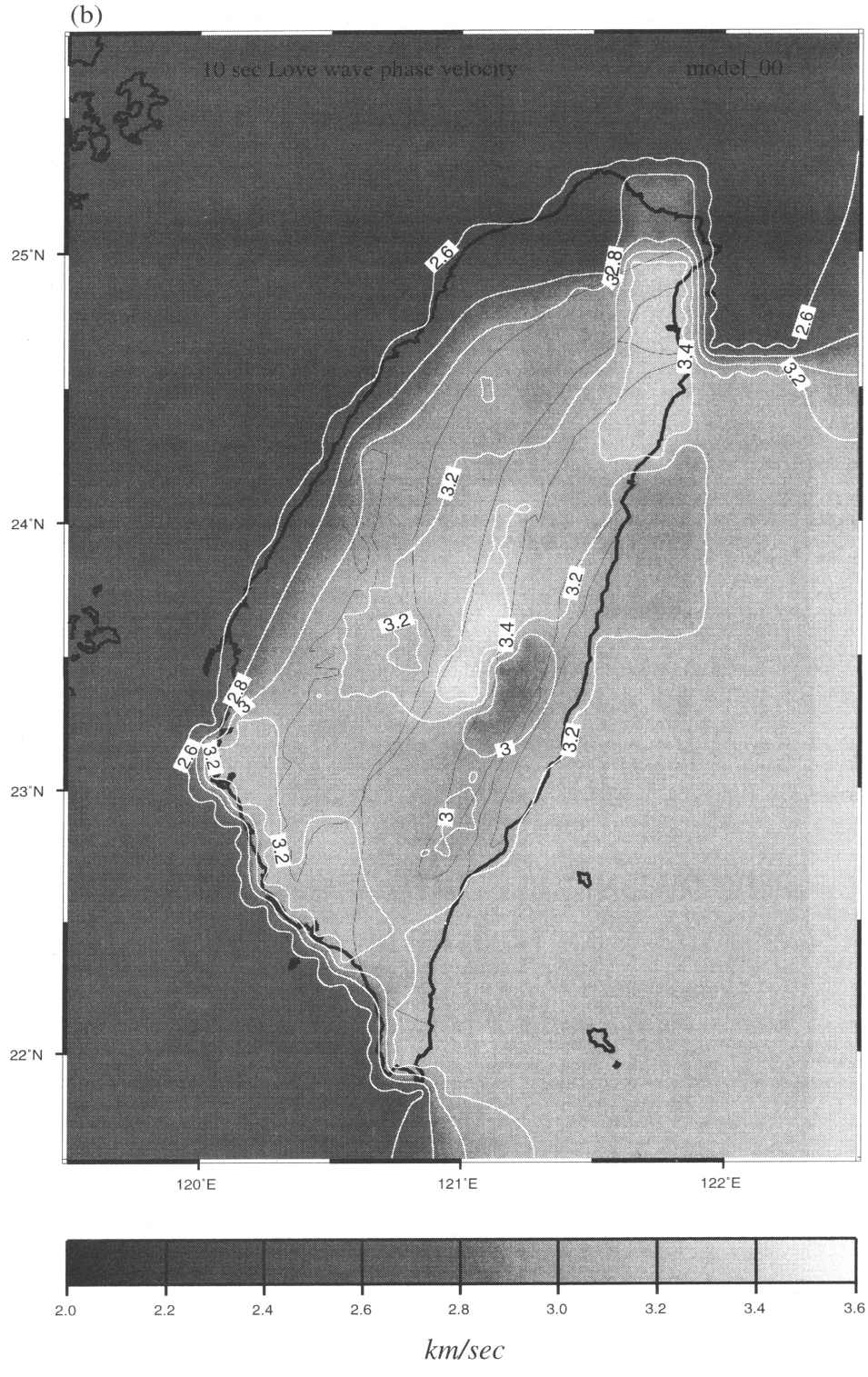

Figure 6b. Corresponding phase velocity distribution of the model in Figure 6a.

The initial focal mechanism of the Tung-Ao earthquake was obtained with first-motion data from the CWBSN weak-motion part of the network. Owing to the relatively sparse coverage by stations for an event in the northeast corner of the seismic network, the uncertainty of the focal mechanism can be substantial. A small discrepancy on focal mechanism may cause significant effect on the radiated wave field [*Kato et al.*, 1993]. A global search procedure is thus used to seek the best fit for the source parameters by maximizing the waveform fit for a fixed velocity model. The search range covers the ±20%

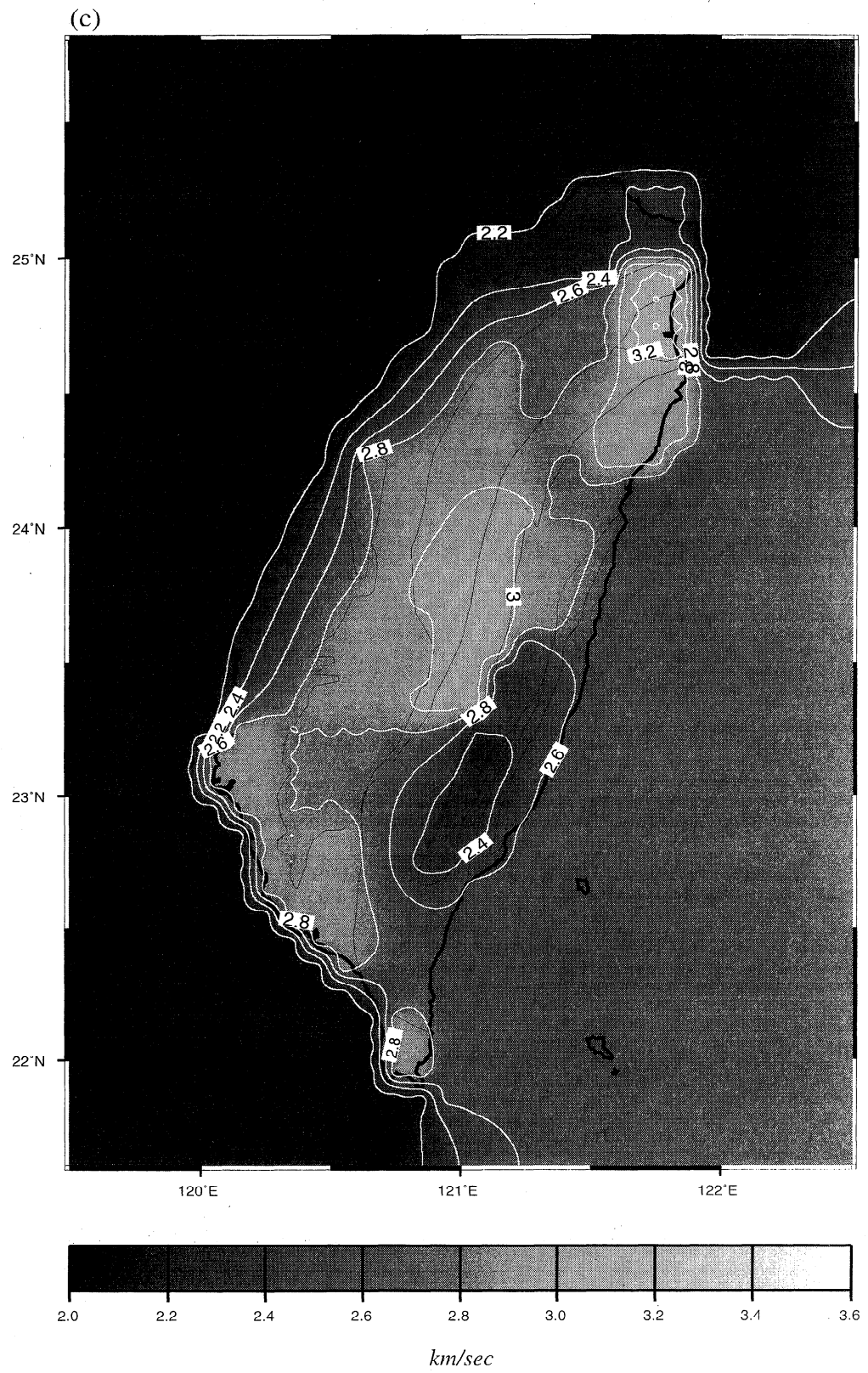

Figure 6c. Group velocity distribution of the initial model in Figure 6a. The WCR and ECR show the highest velocity obviously.

of source parameter perturbation of the source model obtained by the first-motion fault-plane solution.

We focus our attention on waveform simulation of the 10-s-period Love waves because their energy is found to be predominant in the observed ground motions at all stations. The high computational speed in the surface-wave Gaussian beam synthesis has displayed its great advantage here. In an iterative waveform-fitting process, we have gone through thousands of

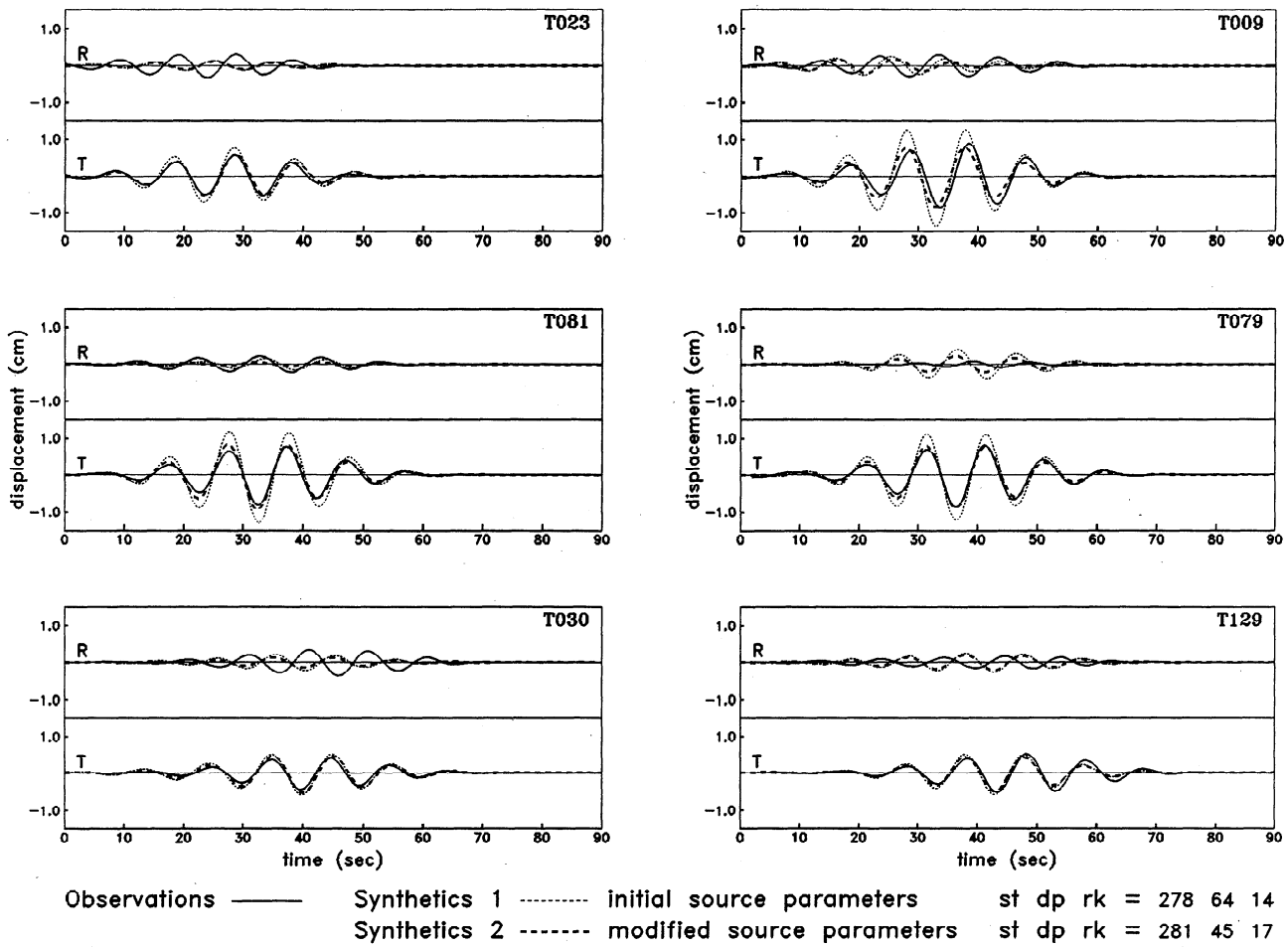

Figure 7. Comparison of waveforms derived from initial source parameters (from first-motion data) and perturbed source parameters based on the final velocity model. Solid lines represent the band-passed observations (displacements), thin dashed lines represent synthetic waveforms using the initial source parameters, and thick dashed lines represent synthetic waveforms using perturbed source parameters as a result of the global search.

iterations nearly interactively. This allows us to zero in on a set of models that provides the best fit of waveforms to most observations. To evaluate the waveform fit, a fitness function [*Zeng and Anderson*, 1996] is calculated, which gives the normalized cross-correlation coefficients of the synthetic seismograms with the data. With a "1" representing a perfect fit for one set of observed synthetic records, the initial model (including velocity and source parameters) gives a fitness function of 6.8 for 18 sets of observed synthetic records of transversal component. We have also made a global search of the source model by perturbing the initial source parameters and comparing the fitness function values, while the velocity model is kept fixed. Sample waveform results (six stations) derived from the initial and final source parameters based on the final velocity model are given in Figure 7. Here the band-passed observations (displacements) are shown by solid lines, synthetic waveforms using the initial source parameters (from first-motion data) are shown by thin dashed lines, and thick dashed lines show synthetic waveforms based on modified source parameters as a result of the global search discussed above. Some improvements are apparent, particularly, in stations T081, T009, and T079. Figure 8 gives the final results of this iterative process. Both the rotated band-passed horizontal displacements of observations and the synthetics derived from initial and final models are displayed. Reasonably good waveform fitting in transversal components has been achieved, as the calculated fitness function value has reached a maximum of 12.5 for most of the observations over a long time window of more than 60 s. Improvement on the waveform fitness for the final model as compared to the initial model is also apparent. For stations (e.g., T028, T029 and T106) with poor waveform fitting the seismograms obviously show smaller amplitudes and their particle polarization deviates from Love-like motions. We conclude that these stations are near the nodal lines, as indicated by the focal mechanism, and perhaps that Rayleigh-like motions, though small, become apparent. For two stations (T042 and T097) located on the area between the regions ECR and COR, the complex geologic structure and rough topography of this region may have severely distorted the waveform, and that results in poor waveform fitting for these two stations. A recent Taiwan island-wide study by *Huang et al.* [1996] also shows that multipathing and lateral boundary reflection in this region cause a very complicated wave field. For other stations, waveform fitting is satisfactory for the transverse component. The corresponding 10-s phase and group velocity maps for the "best fit" waveform results are presented in Figures 9a and 9b,

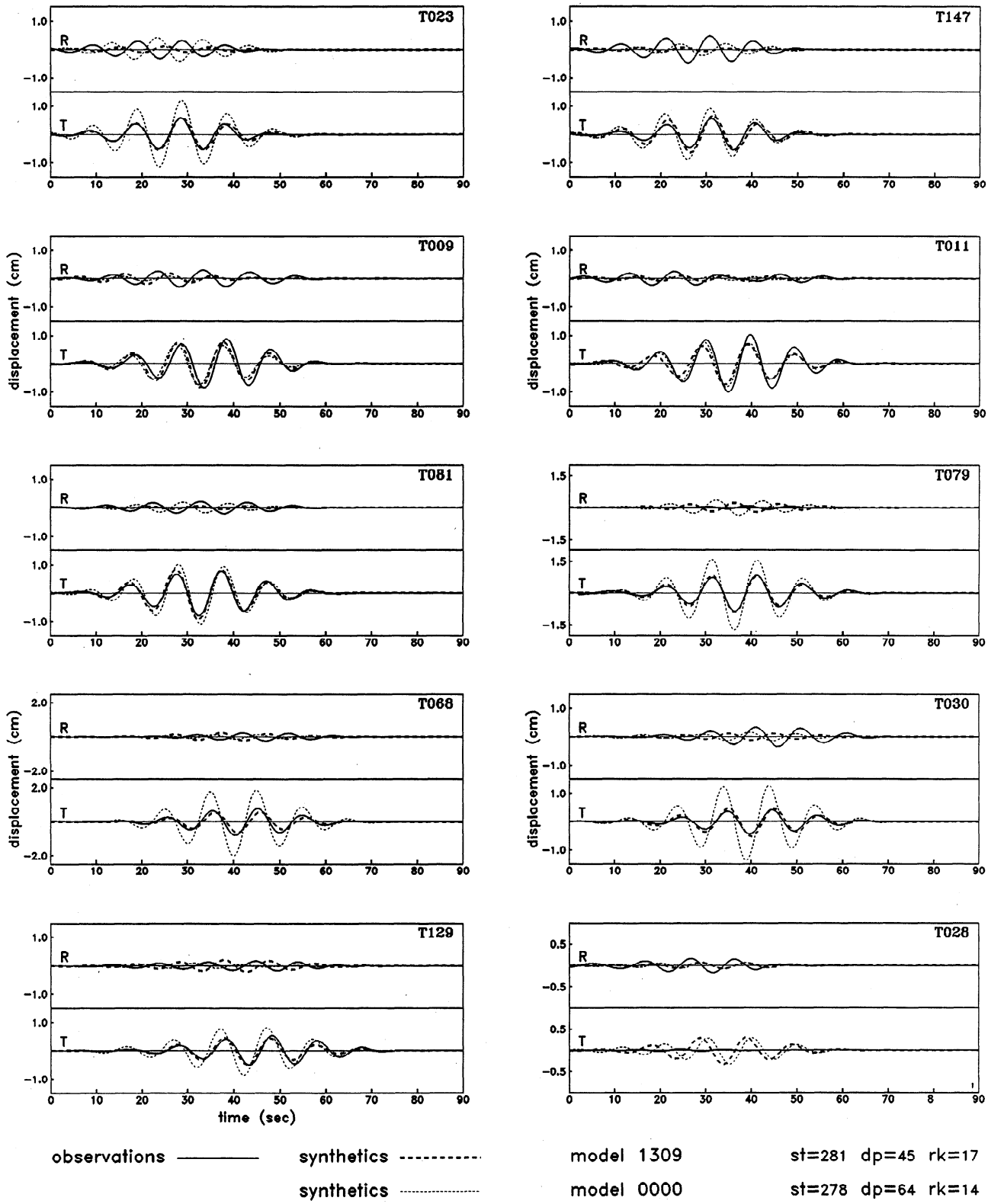

Figure 8. Comparison of our modeling results with observations. The comparison shows that the improvements of waveform fit are obtained through perturbation of the velocity model except for stations located on complex geologic areas or near the nodal lines as indicated by the focal mechanism.

respectively. These can be compared with the Love-wave phase and group velocity maps given in Figures 6b and 6c based on the initial model. These best fit maps basically reflect the gross tectonic features as seen by the 10-s Love waves. The velocity heterogeneity is better modeled than that by the initial model because of the higher sensitivity of waveform synthetics to the lateral velocity variations. From Figures 9a and 9b, high surface-wave velocity zones can be found in the regions ECR,

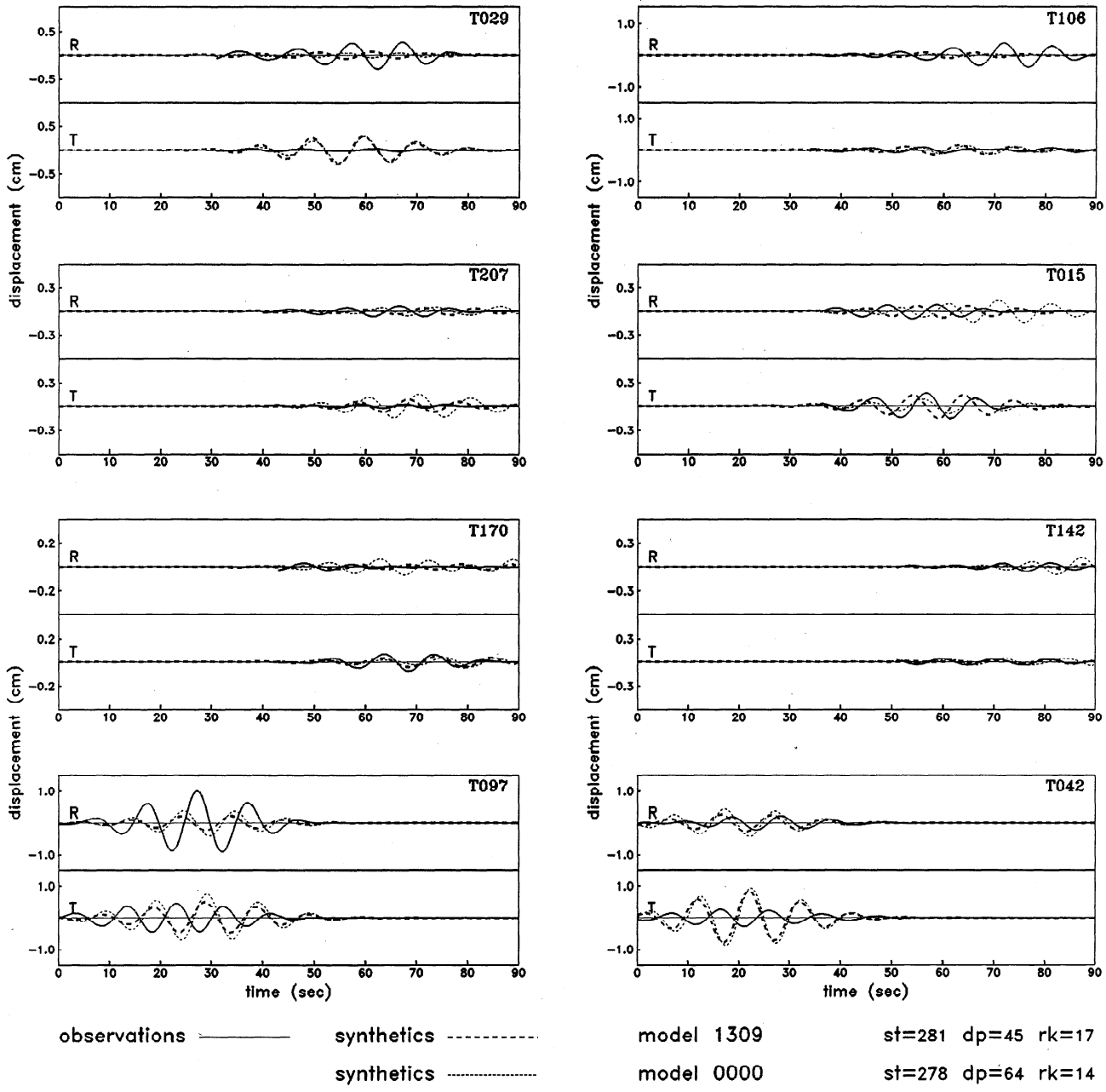

Figure 8. (continued)

COR, and the volcanic area of the northern tip of Taiwan. The resolution of the derived velocity model should be limited owing to sparse station coverage. However, low surface-wave velocity zones coincide with regions having thick sediments such as COP, where station coverage is quite adequate.

A Love-wave ray map (Figure 10) based on the kinematic ray tracing based on phase and group velocity models shown in Figures 9a and 9b is given for the Tung-Ao event. Extensive focusing/defocusing and multipath interference can be found at places that are clearly controlled by the structural heterogeneity. These effects contribute directly to the amplitude variations of our synthetics. Owing to the high phase and group velocity of the ECR and WCR regions, a strong defocusing region for this event is formed around the southern region, COP, where large population and heavy industrialization have developed. As rays propagate through the ECR and WCR regions, these high-velocity zones act like a divergent lens to split the rays away from it. This defocusing phenomenon is demonstrated by stations T032, T095, and T250 (solid squares in Figure 10). All these stations are situated in regions of soft sediments, and therefore of higher site amplification effect. But none of these three stations were even triggered by the Tung-Ao event. With the preset triggering level by CWB, we know that the peak ground acceleration (PGA) there during the Tung-Ao event must have been below 0.01 g, a value much lower than those shown by nearby stations T015, T170, and T207. The nearby station T142, closer to the source, which did trigger, wrote a small record. Hence the crustal heterogeneity is reflected well in the strong-motion amplitude distribution. As an interesting note, the southwest coast of Taiwan has a large population and heavy industrialization, while the Tung-Ao region has frequent large earthquakes. The existence

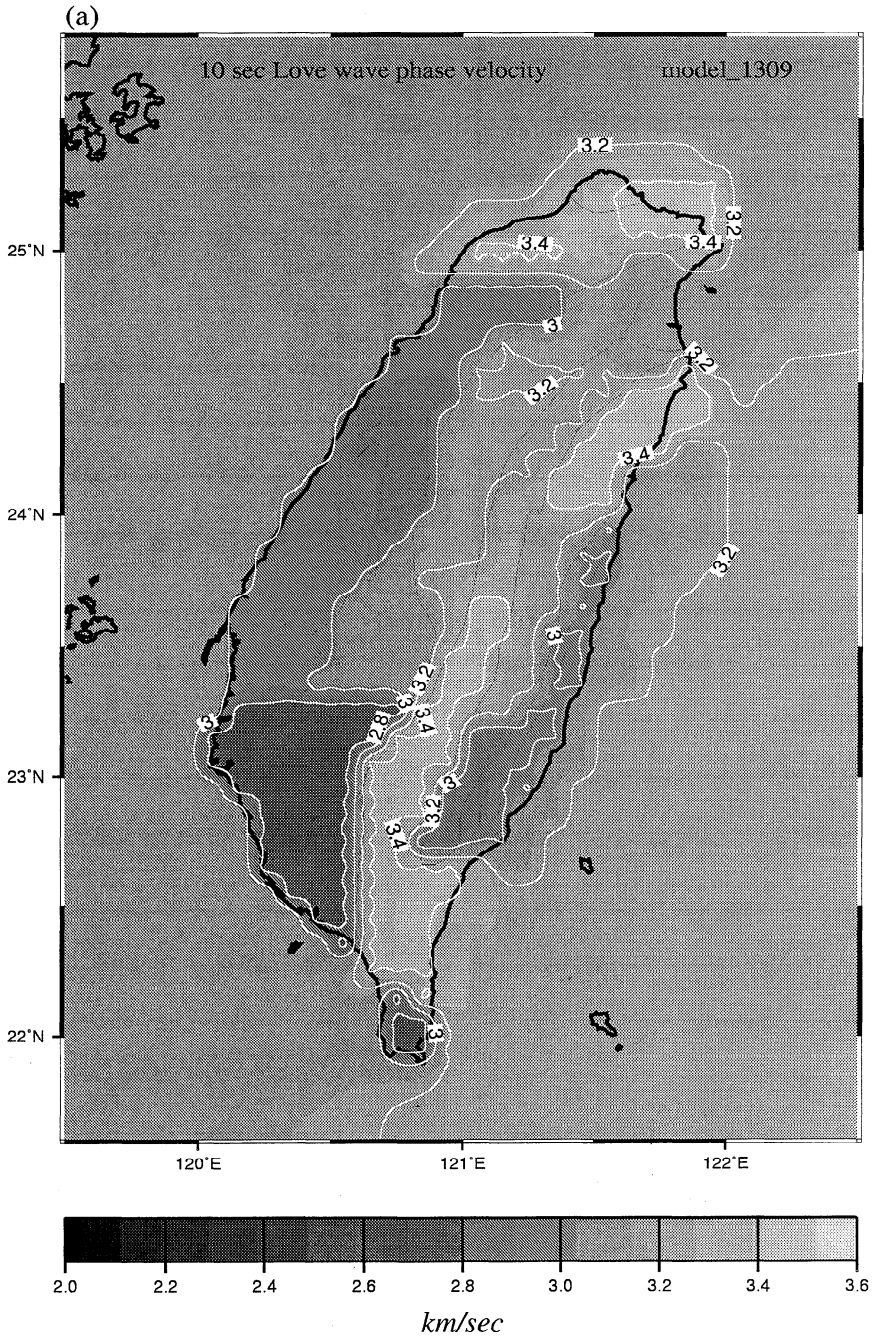

Figure 9a. Phase velocity map of 10-s period Love waves corresponding to our final crustal model from a forward calculation to fit the travel time, amplitude, and waveform information.

of the high-velocity regions WCR and ECR appears to serve as a Love-wave field splitter, which sometimes can effectively protect one of the most populous areas of Taiwan from the onslaught of large-amplitude waves generated by earthquakes from northeast Taiwan and its offshore area.

5. Historic Intensity Data

We shall use the results of surface-wave Gaussian beam calculations to check against available intensity information documented by large historic earthquakes in Taiwan. Instrumental observation in Taiwan began at the turn of this century, with the installation of a dozen or so three-component Wiechert instruments in different cities of Taiwan. These instruments were operated at a fairly low gain with only mechanical magnifications. Their lack of sensitivity became an advantage, however, where on-scale waveform records were obtained when the island was shaken by large earthquakes. Taiwan has gone through a number of large damaging earthquakes in this century. There are two outstanding events that are large enough to give very complete intensity data, one being the 1935 Hsinchu-Taichung earthquake of $M_L = 7.1$, and the other being the 1946 Baihou earthquake of $M_L = 6.8$. In a comprehensive document [*Taipei Observatory*, 1936], outputs of the Wiechert instruments in many observatories are repro-

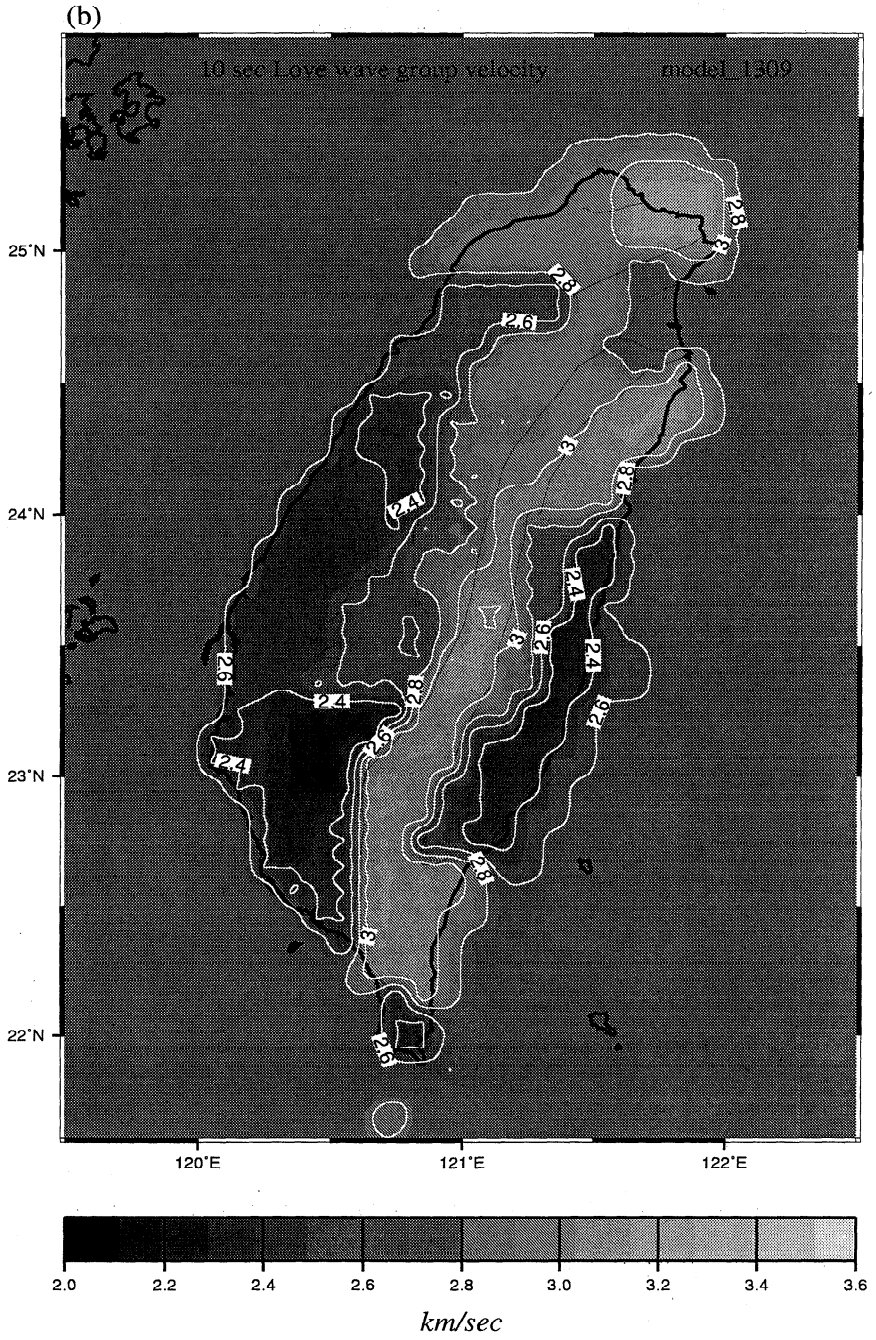

Figure 9b. Same as Figure 9a but for group velocity.

duced. They are beautiful records of long-period displacements, which are generally used to calibrate the rather subjective intensity information. We believe that the reported intensity maps for these two earthquakes in Taiwan are reasonably reliable. For these two earthquakes, surface ruptures were observed, and fault plane solutions were obtained by various studies cited below. We shall use the reported source mechanisms and magnitudes to compute the synthetic displacements, which will then be compared with the reported intensity maps. In the application of the surface-wave Gaussian beam method, the 3-D crustal structure derived in this study will be used.

5.1. The 1935 Hsinchu-Taichung Earthquake

The 1935 Hsinchu-Taichung earthquake is the largest recent event (April 20, 1935, M_L = 7.1) to hit the urbanized area from Hsinchu to Taichung. An extensive field survey was made, and a very comprehensive document was compiled [*Taipei Observatory*, 1936]. There are a number of follow-up studies on this event: relocating the earthquake sequence, and examining the source geometry and its slip distribution [*Lee et al.*, 1985; *Yen*, 1985; *Hsu*, 1985; *Huang and Yeh*, 1992]. To simulate the wave field generated by this event, we need to select proper source parameters. The main rupture of this earthquake is

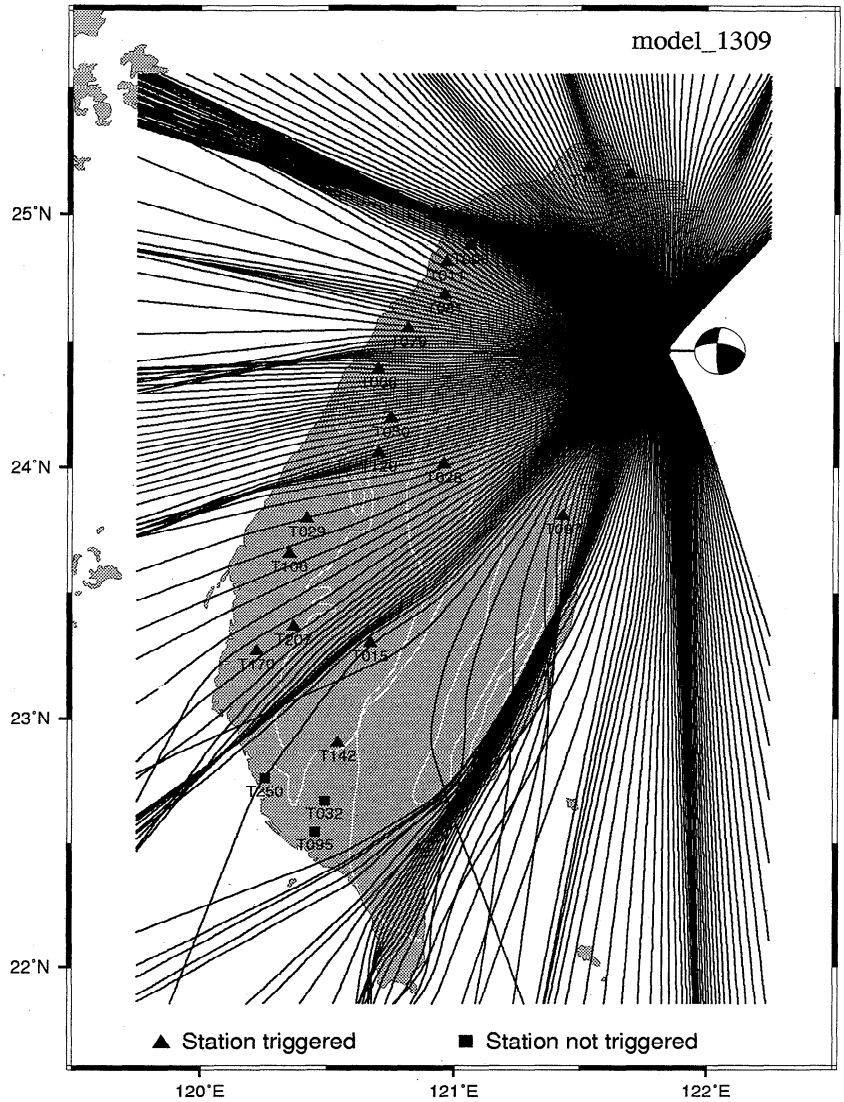

Figure 10. Ray diagram for the final best fit velocity structure. The pronounced focusing/defocusing due to lateral velocity heterogeneity is apparent. Note a distinct defocusing region in southern Taiwan where all three of the nontriggered stations are located.

known to be associated with two segments, the southern segment being an oblique right-lateral strike-slip fault, and the northern segment being a reverse fault. Since the northern segment has released a much larger seismic moment (3.2×10^{26} dyn cm [see *Huang and Yeh*, 1992], we use the source parameters of the northern section in our synthesis. The strike of the northern fault is due north, based on the observed surface deformation and the distribution of aftershocks [*Yen*, 1985]. The dip angle is continuously decreasing from the top (55°) to the bottom (30°) due to the curved fault plane [*Huang and Yeh*, 1992]; an average value of 42° is used in our computation. The rake is very complex, especially in the northern segment; an average value of 85° which corresponds to the major slip occurring on the central part of the fault plane [*Huang and Yeh*, 1992] is used. Results of our simulation are given in a series of figures. Figure 11a gives the ray diagrams of the Love and Rayleigh waves; dominant focusing occurs in regions along the southwestern coast and a narrow band extending from the epicenter to the northeastern coast, particularly for Love waves. These focusing regions unfortunately coincide with cities that were heavily populated even in 1935. This explains why this event was so damaging and also why extensive intensity reports were available then. The defocusing occurs in southeastern Taiwan, due largely to the existence of the regions WCR and ECR serving as a "divergent lens." We have made calculations for an array of 16 field points (T01 through T16, solid angles in Figure 11a) that give a cross section of the propagating wave field. In Figure 11b we give all three-component displacement seismograms with a plot of their corresponding peak amplitudes shown by squares and solid lines in Figure 11c. Note in Figure 11b that the E-W component displacement amplitudes (being primarily Love-like motions) are larger than those of the vertical component, which are primarily Rayleigh-like motions. This indicates that the strong shaking produced by this event as it propagates toward the southern Taiwan region is primarily excited by E-W Love-like motions. Also shown in Figure 11c by diamonds and dashed lines are the corresponding three-component peak displacements computed for a homogeneous crustal model; being free from the effects of lateral heterogeneity, they essentially

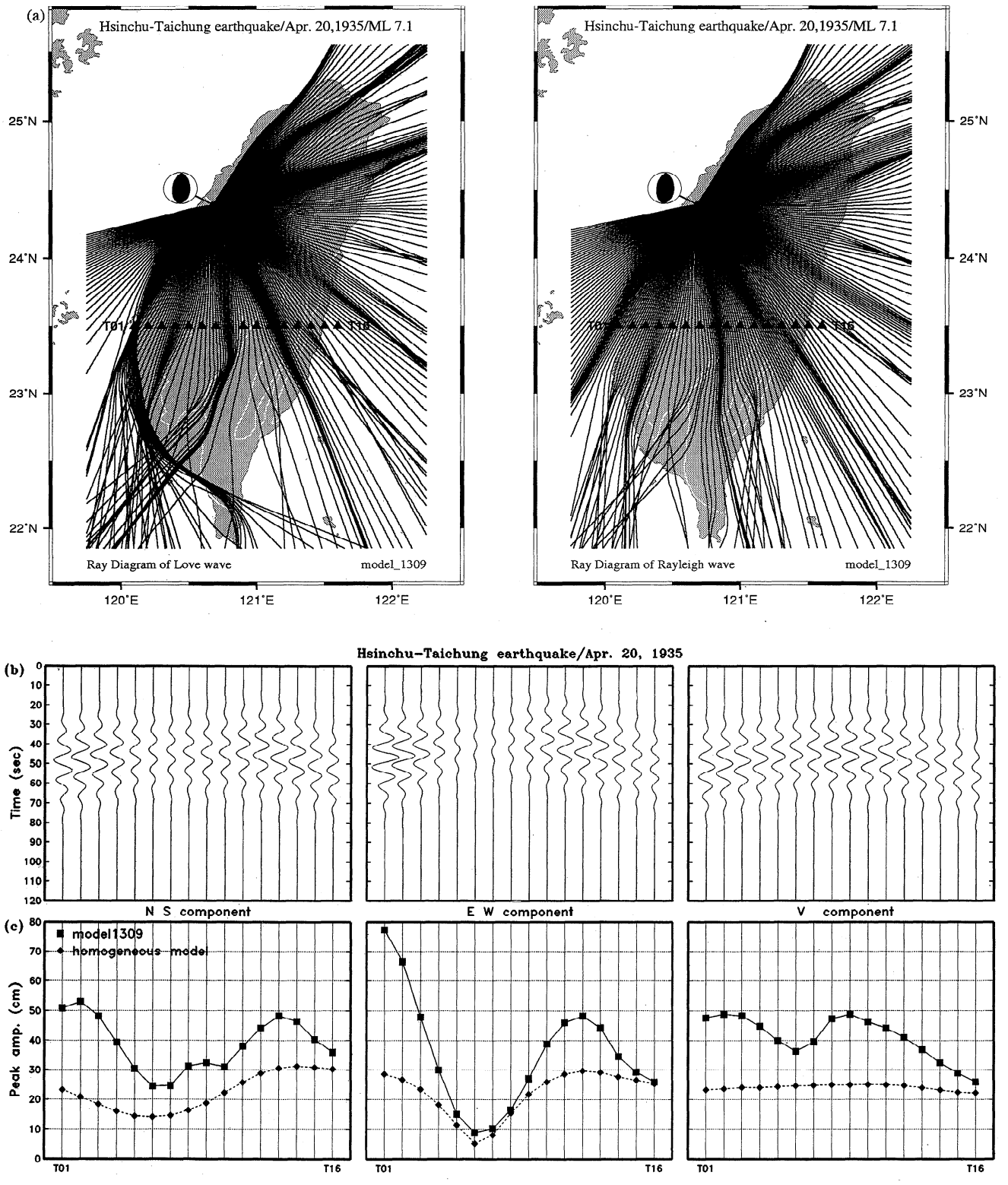

Figure 11. (a) Ray diagram for the Hsinchu-Taichung event (M_L = 7.1, April 20, 1935) for our modified 10-s period surface-wave velocity model. Note the focusing/defocusing areas in southern Taiwan. The solid triangles are field array stations in which the synthetics are calculated to compare the peak amplitudes with the documented intensity distribution. (b) Synthetic waveforms of the array stations. (c) Peak amplitude variations of the field array stations. The solid line and dashed line represent the heterogeneous model and homogeneous model, respectively. (d) Intensity contour map (modified from *Lee et al.* [1985]) of the Hsinchu-Taichung event.

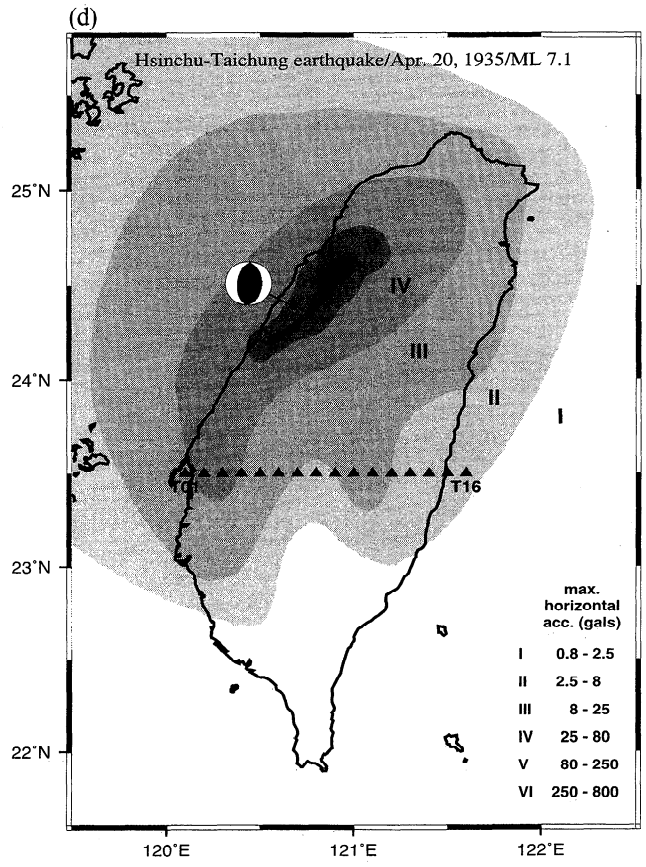

Figure 11. (continued)

represent the earthquake source radiation effect. The four-lobe radiation pattern and the weak radiation at the nodal line are clearly indicated. Since a homogeneous crustal model does not impart distributions to the wave field like a lateral heterogeneous crustal model does, the difference between the squares and diamonds in Figure 11c gives a measure of the propagation effect due to lateral heterogeneity. This difference, varying with the azimuth and due to focusing by the lateral heterogeneity, can cause an amplification of wave motions by as large as 2.5 times. Figure 11d gives the well-documented intensity map in the *Taipei Observatory* (1936) report. Even though the intensity report is a subjective and qualitative report of earthquake shaking, the basic shaking distribution is by and large reproduced by the waveform calculation presented in Figures 11a–11c. This agreement confirms that the source parameters and the crustal structure used in this calculation are reasonable insofar as 10-s surface-wave propagation is concerned.

5.2. The 1964 Baihou Earthquake

Although it had a smaller magnitude of 6.8, the Baihou earthquake (January 18, 1964) was also very damaging to the south central area of Taiwan. It was a shallow thrust-type event, striking roughly N-S with a dip of 45° to east. There are a number of studies [*Hsu and Lu*, 1969; *Lee and Yang*, 1973; *Lin and Tsai*, 1981; *Chang and Yeh*, 1981] that have relocated this event and given these source parameters. Based on the given source parameters and the 3-D crustal structure derived in the current study, the ray diagrams for Love and Rayleigh waves are given in Figure 12a. While focusing is shown by dark beams radiating in many directions, a remarkably strong focusing occurred in a corridor along the SR due to its being bounded by the high-velocity region WCR. This guided wave energy may have produced large intensity at a large distance, even in northern Taiwan (i.e., Taipei). The high-velocity region WCR also deflects the rays and forms an obvious shadow region in northeastern Taiwan. Computed three-component displacement waveforms along two sets of field arrays (B01–B08 and B09–B21) are given in Figure 12b, and peak displacement amplitudes are given as solid squares and solid lines in Figure 12c. Also given in Figure 12c are corresponding peak amplitudes for a laterally homogeneous crustal model, which reflects essentially the source radiation effect. Again, the largest amplitudes are displayed in the E-W component (Love-like motions) at array stations B15 and B16. Pronounced defocusing is shown in the N-S component (Rayleigh-like motions) at array stations B18–B21, while focusing occurs in all array stations in the vertical component and in array stations B12–B16. The reported intensity map, given in Figure 12d, suggests an N-S elongation of the isoseismal contour that is consistent with the computations.

6. Conclusion

Great complexities of strong-motion seismograms are closely controlled by the effects of site, path, and source. For periods longer than 5 s, the effects due to the site variations become insignificant, as the wavelength is much larger than the dimension scale describing a site. Yet these longer period strong motions can be very destructive to large engineering structures, and their impact can project a large (say, 100 km) distance from the source area due to mild attenuation. We have successfully applied the method of surface-wave Gaussian beam calculation to a 3-D crustal structure derived from many recent seismic tomographic studies in Taiwan, where recently installed high-quality digital strong-motion instruments provide numerous large-earthquake recordings that serve as the ground truth checks for the 3-D crustal structure. With adequate source parameters, we have first completed a forward analysis of velocity model perturbations that give excellent fit to observed waveforms generated by the Tung-Ao earthquake of 1994. Our results show that the 3-D structure obtained as the final model of this waveform-fitting process is very adequate; at least it is consistent with the 10-s surface-wave propagation for both Love and Rayleigh waves. Second, based on this improved 3-D crustal model of Taiwan (for 10-s surface waves), we have conducted a study by comparing the computed strong motions in terms of 10-s displacement waveforms and peak amplitudes with the well-documented report of intensity maps for the two largest damaging historic earthquakes. Intensity maps of these two earthquakes are based not only on subjective shaking reports from people and on the building performance, but also on the long-period displacement recordings by the low-gain Wiechert instruments installed in Taiwan at the turn of this century. We have found basic agreements between the synthetic amplitudes with the intensity maps: as the isoseismal contours are shaped both by the source rupture surface, as well as severely affected by the focusing/defocusing effects due to the lateral crustal heterogeneity. The latter is particularly pronounced at large distances away from the source area where the isoseismal contour distortion due to the source should gradually be rounded off. This study concludes that with adequate models of the source and the crustal struc-

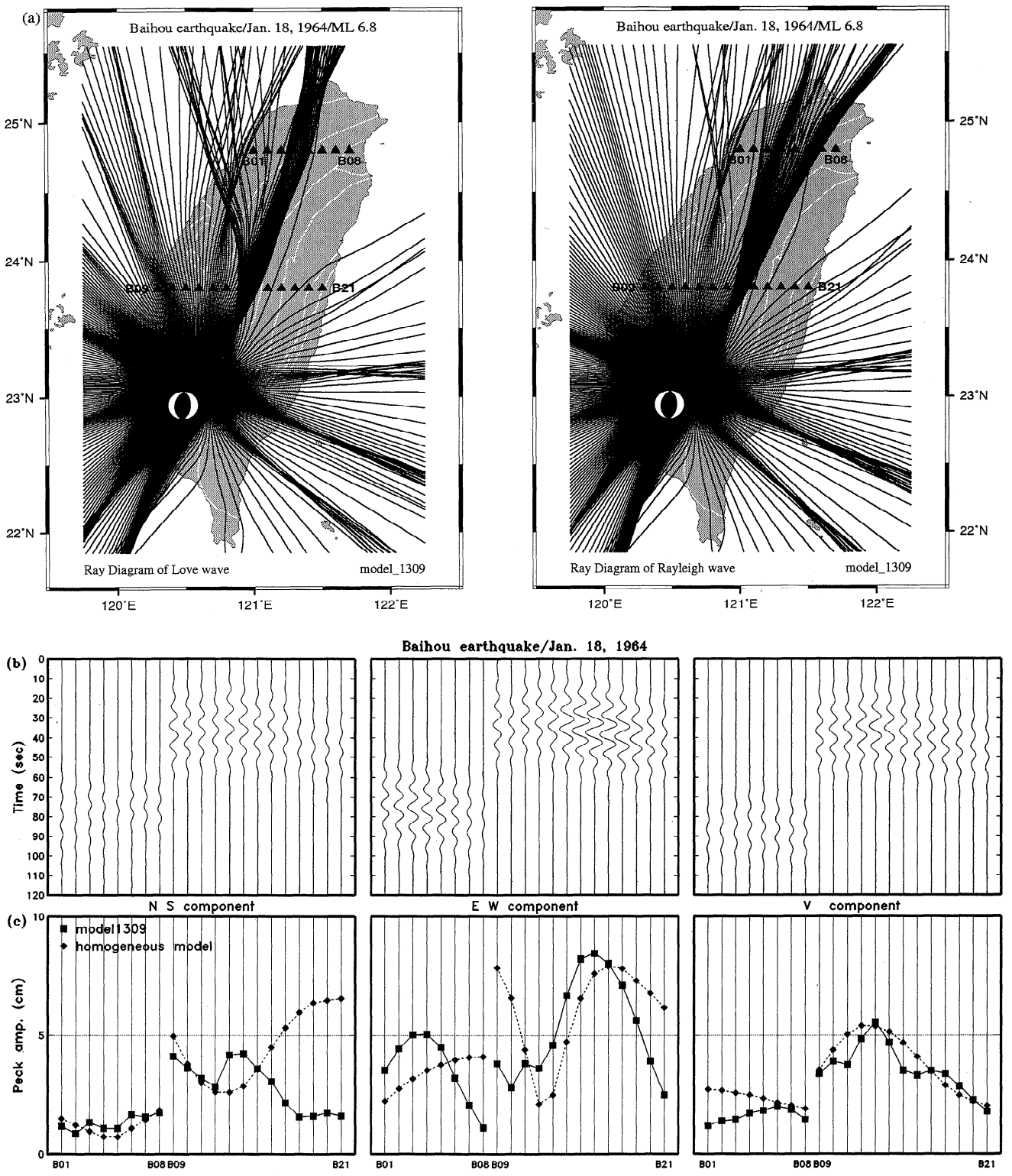

Figure 12. (a) Ray diagram for the Baihou event (M_L = 6.8, January 18, 1964). The channel-guided ray bundle along the SR is due to being bounded by the high-velocity WCR. (b) Synthetic waveforms of the array stations. (c) Peak amplitudes variation of the field array stations. The solid line and dashed line represent the heterogeneous model and homogeneous model, respectively. (d) Intensity contour map (modified from *Hsu and Lu* [1969]) of the Baihou event.

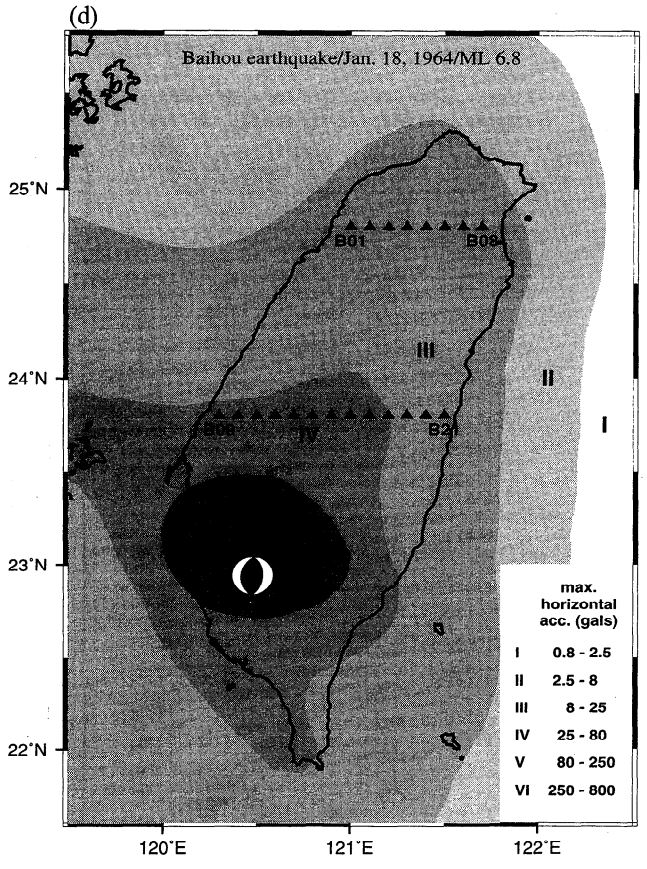

Figure 12. (continued)

ture (i.e., adequate with respect to the wavelength scale of the waveforms under consideration), successful simulations of past observations indicate that prediction of the long-period ground motions is quite possible. While this method does not solve the near-field strong-motion prediction problem, its application to the prediction of the shaking impact to area at a large (say, 100 km) distance from very large events is practical and significant.

Acknowledgments. We wish to thank reviewers J. Tromp and H. Marquering and the associate editor V. Maupin for constructive reviews and T. C. Shin of the Taiwan Central Weather Bureau for operating an excellent broadband, large dynamic range telemetered seismic network. Discussions with our colleagues J. Qu, H. C. Chiu, and H. C. Huang have been most helpful. This research was funded by the National Science Council, Republic of China (contract NSC81-0202-M194-01) and a Central Weather Bureau, Republic of China grant on Earthquake Early Warning and Strong-Motion Instrumentation, as well as (for T.L.T.) by the U.S. Geological Survey (contract 14-08-0001-A0260).

References

Cerveny, V., and I. Psencik, Gaussian beam in two-dimensional elastic inhomogeneous media, *Geophys. J. R. Astron. Soc.*, *72*, 419–435, 1983a.

Cerveny, V., and I. Psencik, Gaussian beam and paraxial ray approximations in three-dimensional elastic inhomogeneous media, *Geophys. J.*, *53*, 1–15, 1983b.

Cerveny, V., M. M. Popov, and I. Psencik, Computation of wave fields in inhomogeneous media—Gaussain beam approach, *Geophys. J. R. Astron. Soc.*, *70*, 109–128, 1982.

Chang, L. S., and Y. T. Yeh, A source model of the Pai-ho, Taiwan earthquake from the inversion of teleseismic body waveforms (in Chinese), *Rep. NSC-69M-0202-02*, Natl. Sci. Counc., Taiwan, 1981.

Chen, C. H., W.-H. Wang, and Y.-H. Yeh, 3-D velocity structure in Taiwan area: A tectonic implication of continent-arc collision (abstract), *Eos Trans. AGU*, *75*(44), Fall Meet. Suppl., 645, 1994.

Ho, C. S., A synthesis of the geological evolution of Taiwan, *Tectonophysics*, *125*, 1–16, 1986.

Ho, M. Y., and T. C. Shin, 3-D velocity structure of western Taiwan, *Meteorol. Bull.*, *40*, 216–234, 1994.

Hsu, H. C., Research on the fault models of the 1935 Hsinchu-Taichung earthquake by geodetic surveying, in *Proceedings of the Commemoration of the 50th Anniversary of the 1935 Hsinchu-Taichung Earthquake*, pp. 45–48, Cent. Weather Bur. and Inst. of Earth Sci., Acad. Sin., Taipei, Taiwan, 1985.

Hsu, M. T., and H. M. Lu, Report on Tainan-Chiayi earthquake of Jan. 18, 1964 (in Chinese), Cent. Weather Bur., Taiwan, 1969.

Huang, B. S., and Y. T. Yeh, Source geometry and slip distribution of the April 20, 1935, Hsinchu-Taichung, Taiwan, earthquake, *Tectonophysics*, *210*, 77–90, 1992.

Huang, B. S., T. L. Teng, C. C. Liu, and T. C. Shin, Excitation of short-period surface waves in Taiwan by the Hyogo-ken Nanbu earthquake of January 17, 1995, *J. Phys. Earth*, *44*, 419–427, 1996.

Kato, K., Y., K. Aki, and T. L. Teng, 3-D simulations of surface wave propagation in the Kanto sedimentary basin, Japan, 1, Application of the surface wave Gaussian beam method, *Bull. Seismol. Soc. Am.*, *83*, 1676–1699, 1993.

Kinoshita, S. H., Fujiwara, T. Mikoshiba, and T. Hoshino, Secondary Love waves observed by a strong-motion array in the Tokyo lowland, *Jpn. J. Phys. Earth*, *40*, 99–116, 1992.

Kudo, K., The contribution of Love waves to strong ground motions, *Proc. Int. Conf. Microzonation*, *2nd*, 765–776, 1978.

Lee, B. H., Y. L. Liu, G. C. Chen, and J. H. Wang, Relocation for the 1935 earthquake sequence, in *Proceedings of the Commemoration of the 50th Anniversary of the 1935 Hsinchu-Taichung Earthquake*, pp. 114–123, Cent. Weather Bur. and Inst. of Earth Sci., Acad. Sin., Taipei, Taiwan, 1985.

Lee, W. H. K., and J. P. Yang, Earthquake activity in the vicinity of Tsengwen reservoir: First progress report, Chinese Earthquake Res. Cent., *Inst. Phys., Acad. Sin.*, *12*, 1–12, 1973.

Lin, M. T., and Y. B. Tsai, Seismotectonics in Taiwan-Luzon area, *Bull. Inst. Earth Sci., Acad. Sinica*, *1*, 51–82, 1981.

Ludwig, W. T., J. E. Nate, and C. L. Drake, Data assembled by John E. Nafe, in *The Sea*, vol. 4, part 1, Wiley-Interscience, New York, 1970.

Ma, K. F., J. H. Wang, and D. Zhao, 3-D seismic velocity structure of the crust and uppermost mantle beneath Taiwan, *Proc. Taiwan Symp. Geophys., 5th*, 147–154, 1994.

Nowack, R., and K. Aki, The 2-D Gaussian beam synthetic method: Testing and applications, *J. Geophys. Res.*, *89*, 1466–1494, 1984.

Qu, J., T. L. Teng, and J. Wang, Modeling of short-period surface-wave propagation in Southern California, *Bull. Seismol. Soc. Am.*, *84*, 596–612, 1994.

Rau, R. T., and F. T. Wu, Tomographic imaging of lithospheric structures under Taiwan, *Earth Planet. Sci. Lett*, *133*, 517–532, 1995.

Roecker, S. W., Y. H. Yeh, and Y. B. Tsai, Three-dimensional *P* and *S* wave velocity structure beneath Taiwan: Deep structure beneath an arc-continent collision, *J. Geophys. Res.*, *92*, 10,547–10,570, 1987.

Seo, K., Earthquake motions modulated by deep soil structure of Tokyo, *Proc. Jpn. Earthquake Eng. Symp., 5th*, 281–287, 1978.

Shin, T. C., Progress summary of the Taiwan strong motion instrumentation program, in *Symposium on Taiwan Strong Motion Instrumentation Program*, pp. 1–10, Cent. Weather Bur., Taipei, Taiwan, 1993.

Taipei Observatory, The Great Hsinchu-Taichung Earthquake Report, 160 pp., Taiwan, 1936.

Tanaka, T., S. Yoshizawa, and Y. Osawa, Characteristics of strong earthquake ground motion in the period range from 1 to 15 seconds (in Japanese with English abstract), *Bull. Earthquake Res. Inst. Tokyo Univ.*, *54*, 629–655, 1979.

Tsai, Y. B., Plate subduction and the Plio-Pleistocene orogeny in Taiwan, *Petrol. Geol. Taiwan*, *15*, 1–10, 1978.

Tsai, Y. B., Seismotectonics of Taiwan, *Tectonophysics*, *125*, 17–37, 1986.

Tsai, Y. B., T. L. Teng, J. M. Chiu, and H. L. Liu, Tectonic implications of the seismicity in the Taiwan region, *Mem. Geol. Soc. China*, *2*, 13–42, 1977.

Yeh, Y. H., and Y. B. Tsai, Crustal structure of central Taiwan from

inversion of *P*-wave arrival times, *Bull. Inst. Earth Sci. Acad. Sin.*, *1*, 83–102, 1981.

Yen, C. B., Retrospect of the field survey after the 1935 Hsinchu-Taichung earthquake, in *Proceedings of the Commemoration of the 50th Anniversary of the 1935 Hsinchu-Taichung Earthquake*, pp. 11–17, Cent. Weather Bur. and Inst. of Earth Sci., Acad. Sin., Taipei, Taiwan, 1985.

Yokota, H., S. Kataoka, and T. Tanaka, Characteristics of strong earthquake ground motion in period of 1 to 15 seconds observed in Tokyo (in Japanese), *Proc. Jpn. Earthquake Eng. Symp.*, *7th*, 193–198, 1986.

Yomogida, K., and K. Aki, Waveform synthesis of surface waves in a laterally heterogeneous earth by the Gaussian beam method, *J. Geophys. Res.*, *90*, 7665–7688, 1985.

Yomogida, K., and K. Aki, Amplitude and phase data inversion for phase velocity anomalies in the Pacific Ocean basin, *Geophys. J. R. Astron. Soc.*, *88*, 161–204, 1987.

Zeng, Y., and J. G. Anderson, A composite source model of the 1994 Northridge earthquake using genetic algorithms, *Bull. Seismol. Soc. Am.*, *86*, S71–S83, 1996.

C.-H. Chen and Y.-C. Gung, Institute of Seismology, National Chung Cheng University, Chia-Yi, Taiwan 621. (e-mail: seichen@eq.ccu.edu.tw)

T.-L. Teng, Department of Earth Sciences, University of Southern California, Los Angeles, CA 90089-0740. (e-mail: lteng@coda.usc.edu)

(Received March 31, 1997; revised January 9, 1998;
accepted February 17, 1998.)